

An Enhanced Framework for Wave Reflection from a Periodically Rough Boundary

Fei Yin^a, Shixian Liu^a, Alexander A. Barinov^a, Vladimir I. Khvesyuk^{a,*}

^a*Department of Thermophysics, Bauman Moscow State Technical University, 2nd Baumanskaya 5, Moscow, 105005, Russian Federation*

Abstract

This paper presents an updated comprehensive model for specular reflection from a periodically rough boundary. The model accounts for both phase loss and angular deviations of the reflected wave, enabling a statistical evaluation of the specular reflection probability as a function of wavelength, roughness amplitude, roughness period, and incident angle. Notably, the model reveals oscillatory behavior in the specular reflection probability within the high-frequency regime. The proposed formulation is further incorporated into the Ziman model and applied in Monte Carlo simulations to evaluate thermal conductivity.

Keywords: specular reflection model, wave, thermal conductivity, roughness, Monte Carlo simulation

*Corresponding author
Email address: khvesyuk@bmstu.ru (Vladimir I. Khvesyuk)

1. Introduction

Boundary roughness plays a critical role in nanoscale thermal transport by influencing phonon boundary scattering and, consequently, thermal conductivity[1]. At this scale, the distinction between specular and diffuse phonon reflection becomes particularly important: specular reflection preserves phonon momentum and sustains heat flux, whereas diffuse scattering randomizes phonon trajectories and impedes thermal transport. Accurate modeling of surface roughness is therefore essential for understanding and predicting thermal behavior in nanostructured materials [2, 3].

Among the existing models, the concept of a specular reflection parameter is widely used to quantify the probability of phonons undergoing specular versus diffuse scattering at rough surfaces[4]. Casimir's model [5] assumes fully diffuse reflection, while Ziman [6] introduced a wavelength-dependent specularity parameter p , which relates the phonon wavelength to the root-mean-square (RMS) surface roughness. However, Ziman's model assumes normal incidence and neglects the effect of the roughness correlation length. Soffer [7] later extended the theory to arbitrary incidence angles, although it still assumes an infinitely long correlation length.

Recent studies have refined the specularity model by incorporating wavelength dependence and RMS roughness, resulting in improved agreement with experimental data [8–12]. However, experimental evidence shows that the correlation length also plays a significant role. Lim *et al.* [13] demonstrated that the specularity parameter p strongly depends on both RMS roughness and correlation length, while Ravichandran *et al.* [14] highlighted its pronounced wavelength dependence. To account for finite correlation lengths, Maznev *et al.* [15] proposed a modified model, though it remains limited to normal incidence. Many subsequent studies continued to simplify phonon-boundary interactions by treating the specularity parameter p as a constant, independent of phonon wavelength or surface morphology. This oversimplification fails to capture the diverse scattering behavior of phonons with different wavelengths and incident angles.

These limitations highlight a pressing need for more comprehensive models that accurately describe phonon–surface interactions across a range of geometries, wavelengths, and surface morphologies. Such models are essential for a deeper understanding of nanoscale heat conduction mechanisms, particularly in regimes where confinement effects, ballistic transport, and coherent phonon interference become significant. Without resolving these fundamen-

tal issues, it remains challenging to elucidate the interplay of particle-like and wave-like phonon behavior and to rationally design nanostructures with tailored thermal properties for next-generation thermal management applications.

Periodic roughness has also been experimentally realized in nanostructures [16], further revealing limitations of existing models. When periodic surface features are present, both Lorentz gas simulations [17] and molecular dynamics studies [18] report a non-monotonic dependence of thermal conductivity on roughness amplitude. These findings underscore the importance of wave effects in phonon transport—effects neglected by conventional particle-based models, which typically predict a monotonic decrease in conductivity with increasing roughness. Because phonons have finite wavelengths, their interaction with periodic structures is highly sensitive to the relationship between wavelength and surface modulation, leading to constructive or destructive interference.

The Ziman–Soffer model, developed for randomly rough surfaces with infinite correlation length, fails to capture these effects and is therefore inadequate for periodic structures. A more comprehensive theoretical framework is needed—one that incorporates phonon wavelength, incidence angle, and the geometric parameters of periodic roughness. Moreover, such a model should account not only for boundary scattering but also for both specular and backward reflections occurring at interfaces [19].

In this work, we introduce an improved reflection model for phonons interacting with periodically rough boundaries. The surface is represented by a sinusoidal profile, and the reflection behavior is derived based on statistical phase disruption and angular deviation of the reflected waves. The resulting expression yields a specularity parameter that depends on both wavelength and angle, explicitly incorporating roughness amplitude and period. This model generalizes the classical Ziman approach and is readily applicable to Monte Carlo simulations. We apply the model to compute the thermal conductivity of thin films with periodic surface features, revealing non-monotonic trends consistent with wave interference effects.

2. Methodology

In this study, a theoretical and numerical framework is developed to describe phonon specular reflection from periodically rough surfaces, which are

commonly encountered in modern nanofabrication technologies. The surface profile is assumed to follow a deterministic sinusoidal function:

$$h(x) = A \sin\left(\frac{2\pi}{L}x\right), \quad (1)$$

where A is the amplitude and L is the spatial period of the boundary roughness.

2.1. Extended Ziman Model for a Periodically Rough boundary

As shown in Fig. 1a, when a plane wave with wavelength λ is incident on a rough boundary at angle θ , the height variation introduces a position-dependent phase shift [20]:

$$\Delta\varphi(x) = \frac{4\pi}{\lambda}h(x)\cos\theta, \quad (2)$$

The coherent amplitude of the specular reflection is then obtained by averaging the phase factor over one boundary period:

$$A_{\text{coh}} = \langle e^{i\Delta\varphi} \rangle = \frac{1}{L} \int_0^L e^{i\Delta\varphi(x)} dx = J_0\left(\frac{4\pi A \cos\theta}{\lambda}\right), \quad (3)$$

where J_0 is the zeroth-order Bessel function of the first kind. The derivation of this expression is provided in Appendix A.

The specular reflection probability (also referred to as the specularity parameter) is then given by:

$$p = |A_{\text{coh}}|^2 = J_0^2\left(\frac{4\pi A \cos\theta}{\lambda}\right). \quad (4)$$

2.2. An Updated Comprehensive Model

The Ziman and Soffer models, along with the model in the previous section, consider only surface roughness amplitude while ignoring the horizontal scale of roughness—referred to as the *roughness period* in this study. When the period is explicitly included, the local surface inclination must be accounted for. With respect to the local surface normal, the reflection angle equals the incident angle; however, when measured relative to the vertical axis, the reflection angle varies with position, as illustrated in Fig. 1b.

Thus, this updated model incorporates both the local phase difference and the deflection of the reflected wave direction. Since we are interested

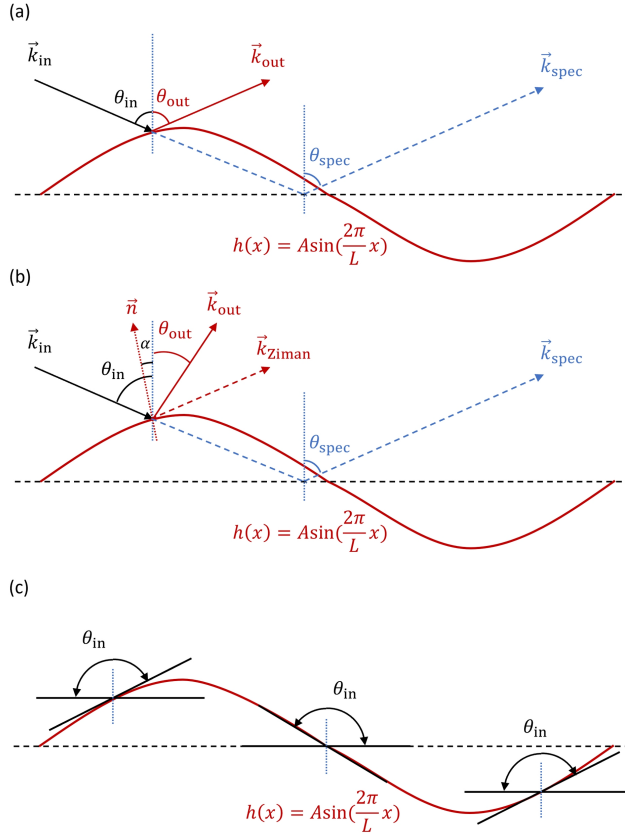


Figure 1: (a) Extended Ziman model based on a periodically rough boundary; (b) Updated comprehensive model including both roughness period and amplitude; (c) Diagram showing valid incident angle ranges at different boundary positions.

in the coherent amplitude along the mirror reflection direction, the reflected amplitude must be projected accordingly. The resulting expression is:

$$A_{coh} = \frac{1}{L} \int_0^L e^{i\Delta\varphi(x)} e^{i(\vec{k}_{out}(x)-\vec{k}_{spec}) \cdot \vec{r}(x)} dx, \quad (5)$$

where the integration is performed along the boundary profile, parameterized by the horizontal coordinate x , which spans one spatial period of the surface roughness. The vector $\vec{k}_{out}(x)$ represents the locally reflected wavevector, which depends on the local surface slope. In contrast, $\vec{k}_{spec}(x)$ corresponds to the ideal specular reflection wavevector from a perfectly flat surface.

$$\vec{k}_{\text{out}}(x) = \frac{2\pi}{\lambda} \begin{pmatrix} \sin \theta_{\text{out}}(x) \\ \cos \theta_{\text{out}}(x) \end{pmatrix}, \quad (6)$$

$$\vec{k}_{\text{spec}} = \frac{2\pi}{\lambda} \begin{pmatrix} \sin \theta_{\text{spec}} \\ \cos \theta_{\text{spec}} \end{pmatrix}, \quad \theta_{\text{spec}} = -\theta_{\text{in}}, \quad (7)$$

The vector $\vec{r}(x)$ represents the local position on the rough boundary:

$$\vec{r}(x) = \begin{pmatrix} x \\ h(x) \end{pmatrix}, \quad (8)$$

where x is the in-plane coordinate along the surface and $h(x)$ is the corresponding surface height.

The term $(\vec{k}_{\text{out}}(x) - \vec{k}_{\text{spec}}) \cdot \vec{r}(x)$ describes the geometric phase shift between the actual and ideal reflected waves. This phase difference arises because the direction of reflection varies locally due to surface roughness.

Each reflected wave at position x carries a phase $e^{i\Delta\varphi(x)} \cdot e^{i\vec{k}_{\text{out}}(x) \cdot \vec{r}(x)}$, but since we are only interested in its component along the specular direction, we apply a projection by multiplying $e^{-i\vec{k}_{\text{spec}} \cdot \vec{r}(x)}$, which leads to the final form: $e^{i\Delta\varphi(x)} \cdot e^{i(\vec{k}_{\text{out}}(x) - \vec{k}_{\text{spec}}) \cdot \vec{r}(x)}$.

Locally reflected wavevector $\vec{k}_{\text{out}}(x)$ is computed by reflecting the incident wave vector \vec{k}_{in} with respect to the local normal vector $\vec{n}(x)$ [21]:

$$\vec{k}_{\text{out}}(x) = \vec{k}_{\text{in}} - 2 \left[\vec{k}_{\text{in}} \cdot \vec{n}(x) \right] \vec{n}(x). \quad (9)$$

where, the local normal vector $\vec{n}(x)$ is

$$\vec{n}(x) = \frac{1}{\sqrt{1 + h'(x)^2}} \begin{pmatrix} -h'(x) \\ 1 \end{pmatrix}, \quad (10)$$

and incident wave vector is:

$$\vec{k}_{\text{in}} = \frac{2\pi}{\lambda} \begin{pmatrix} \sin \theta_{\text{in}} \\ -\cos \theta_{\text{in}} \end{pmatrix}. \quad (11)$$

It is important to note that at certain surface positions, the incident angle cannot be arbitrary. In some cases, the wave may be blocked or yield no physical reflection. Therefore, a geometric constraint must be enforced: the incident angle must be greater than the local tilt angle at the point of interaction, as illustrated in Fig. 1c.

2.3. Monte Carlo Simulation

To evaluate the thermal effects of specular and diffuse scattering, we further implement a Monte Carlo (MC) simulation of phonon transport based on the Boltzmann Transport Equation (BTE) under the relaxation time approximation:

$$\frac{\partial f}{\partial t} + \vec{v}_g \cdot \nabla_{\vec{r}} f = \left(\frac{\partial f}{\partial t} \right)_{\text{scatt}}, \quad (12)$$

where $f(\vec{r}, \vec{k}, t)$ is the phonon distribution function and $\vec{v}_g = \nabla_{\vec{k}}\omega(\vec{k})$ is the phonon group velocity.

In this method, phonon bundles are initialized according to the Bose–Einstein distribution and are propagated through the simulation domain. Each phonon particle is assigned a wave vector \vec{k} , polarization branch p , group velocity \vec{v}_g , and angular frequency ω , and moves ballistically between scattering events[12, 22].

Boundary scattering plays a crucial role in nanostructures. When a phonon encounters a boundary, it may reflect specularly or diffusely depending on the local roughness, incident angle, and wavelength. The specularity parameter $p(A, L, \lambda, \theta) \in [0, 1]$ defines the probability of specular reflection. A random number $R \in [0, 1]$ is drawn to determine the reflection type:

- If $R < p$, the phonon reflects specularly (mirror-like).
- If $R \geq p$, the phonon reflects diffusely, with a randomized outgoing direction.

Scattering events, phonon-phonon interactions, and boundary collisions are handled probabilistically, and energy exchange is tracked within spatial cells. The total phonon energy in each cell is then converted to a local temperature via [23–25]:

$$E_{\text{cell}} = \sum_i N_i \hbar \omega_i \Rightarrow T = T(E), \quad (13)$$

where N_i is the number of particles in mode i , and $T(E)$ is computed through inversion of the Bose–Einstein distribution.

3. Results and Discussion

The corresponding local reflection angle $\theta_{\text{out}}(x)$, measured with respect to the vertical axis, is extracted from the components of $\vec{k}_{\text{out}}(x)$. The relationship between the calculated $\theta_{\text{out}}(x)$, the incident angle θ_{in} , and the reflection point position x is illustrated in Fig. 2.

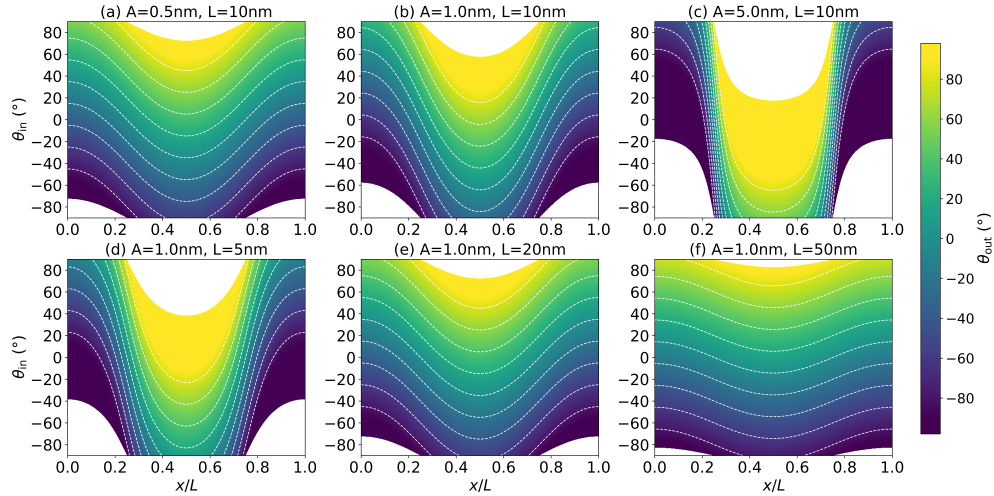


Figure 2: Relationship between reflection angle, incident angle, and collision position for different roughness configurations: (a) amplitude 0.5 nm, period 10 nm; (b) amplitude 1.0 nm, period 10 nm; (c) amplitude 5.0 nm, period 10 nm; (d) amplitude 1.0 nm, period 5 nm; (e) amplitude 1.0 nm, period 20 nm; (f) amplitude 1.0 nm, period 50 nm.

The blank regions in Fig. 2 correspond to incident angles that are not physically meaningful, as previously analyzed in Fig. 1c. These regions indicate cases where the incoming wave is either blocked or does not lead to a valid reflection due to the steepness of the surface.

It is evident that the relationship between the reflection angle and the incident angle varies depending on the collision point along the rough surface. This variation illustrates the physical nature of diffuse reflection: the steeper the contour, the lower the specular reflectivity; the flatter the contour, the higher the specular reflectivity.

Figures 2a–c show that for a fixed roughness period, increasing the amplitude results in steeper contours and thus reduced specular reflection. Conversely, Figures 2d–f demonstrate that for a fixed amplitude, increasing the period leads to flatter contours and enhanced specular reflection. These trends are consistent with physical expectations.

The results of the specular reflection probability as functions of wavelength and angle of incidence are presented in Fig. 3. Figures 3a–c are based on the extended Ziman model, which accounts only for the roughness amplitude, set to 0.5, 1.0, and 5.0 nm, respectively. Figures 3d–i are obtained from the updated comprehensive model, which considers both the roughness amplitude and period. In particular, Figs. 3d–f correspond to a fixed roughness period of 10 nm, with amplitudes of 0.5, 1.0, and 5.0 nm, respectively. Figs. 3g–i correspond to a fixed roughness amplitude of 1.0 nm, with roughness periods of 5, 20, and 50 nm, respectively.

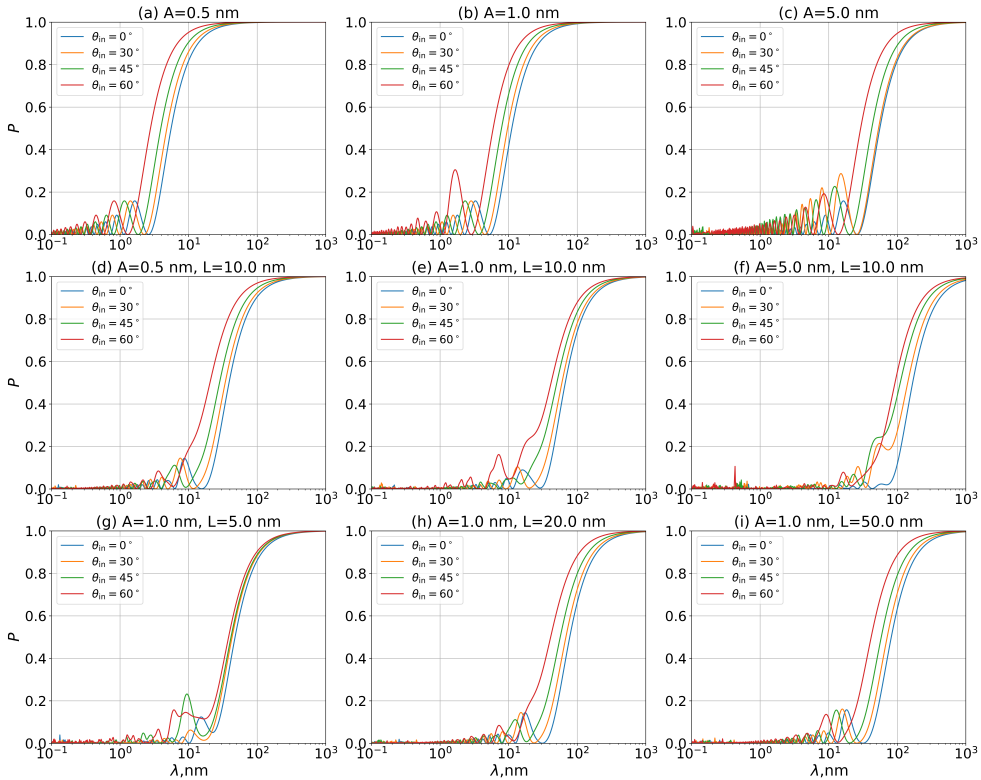


Figure 3: Specular reflection probability p as a function of wavelength λ and incident angle θ_{in} . (a–c) Extended Ziman model with roughness amplitudes $A = 0.5, 1.0$, and 5.0 nm, neglecting the effect of roughness period. (d–f) Updated model with fixed period $L = 10$ nm and amplitudes $A = 0.5, 1.0$, and 5.0 nm. (g–i) Updated model with fixed amplitude $A = 1.0$ nm and periods $L = 5, 20$, and 50 nm.

From Figs. 3a–c and 3d–f, it is evident that increasing the roughness amplitude significantly reduces the specular reflection probability. This is due

to the stronger local phase differences and larger angular deflections caused by steeper surfaces, which enhance diffuse scattering. In contrast, as shown in Figs. 3a–c and 3g–i, increasing the roughness period has a comparatively minor effect on specular reflection, particularly in the long-wavelength region.

However, a notable phenomenon appears in the short-wavelength region: oscillations in the specular reflection probability as a function of wavelength. This behavior arises from the interference effects among reflected wavelets from different surface points. At short wavelengths, the phase differences between adjacent points become more sensitive to surface geometry, leading to alternating constructive and destructive interference in the mirror direction. These oscillations are especially pronounced when the roughness is periodic, effectively acting like a phase diffraction grating.

In the context of phonon transport, these oscillatory features suggest that specular reflection alone is not a smooth function of wavelength, especially in the high-frequency regime. As such, a more accurate evaluation of its influence on thermal transport should be based on cumulative effects, such as those captured in Monte Carlo simulations or direct thermal conductivity calculations. This would account not only for angle-dependent scattering but also for energy transport across all phonon modes.

The in-plane thermal conductivity of films with rough surfaces, calculated using Monte Carlo simulations, is presented in Fig. 4. These results correspond to films of varying thickness H . As shown in Fig. 4a, when the roughness period L is fixed at 0.5 nm and 6 nm, the thermal conductivity exhibits a monotonic decrease with increasing roughness amplitude. For extremely small amplitudes ($A < 0.03$ nm) and large amplitudes ($A > 0.4$ nm), the influence of L becomes negligible, yielding nearly identical values for different roughness periods. Figure 4b illustrates the case where the roughness amplitude is fixed at 0.1 nm and 0.4 nm. When $A = 0.1$ nm, the thermal conductivity initially decreases and subsequently increases as L increases. In contrast, for $A = 0.4$ nm, the effect of L is small, resulting in an almost flat dependence.

When A takes intermediate values (0.03–0.4 nm), the thermal conductivity exhibits a non-monotonic dependence on L . This behavior can be explained as follows: when the roughness period L approaches a small value, the characteristic size of the surface roughness becomes smaller than the wavelengths of most phonons. As a result, phonons become less sensitive to the roughness features, leading to reduced scattering and an increase in thermal conductivity. On the other hand, when L becomes large while main-

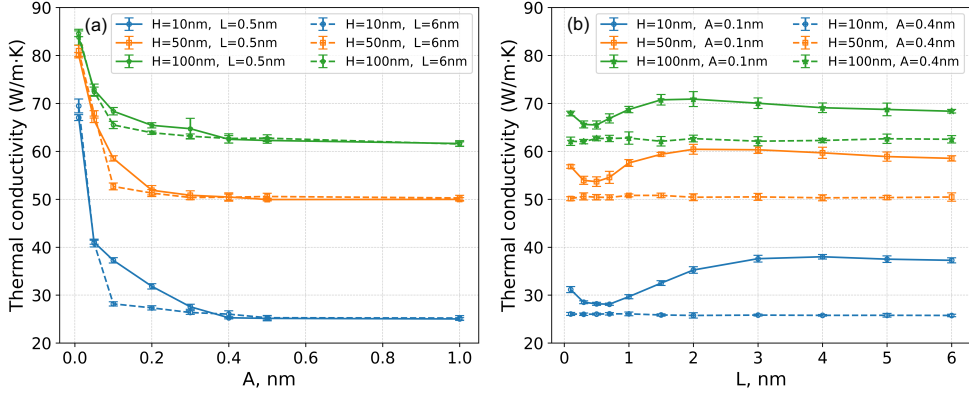


Figure 4: In-plane thermal conductivity of films with varying thickness H , obtained from Monte Carlo simulations. (a) Dependence of thermal conductivity on roughness amplitude A for fixed roughness periods $L = 0.5$ nm and $L = 6.0$ nm. (b) Dependence of thermal conductivity on roughness period L for fixed amplitudes $A = 0.1$ nm and $A = 0.4$ nm.

taining a fixed amplitude, the surface becomes less steep, resulting in smaller deflection angles during phonon reflection. This leads to reduced energy loss and, consequently, higher thermal conductivity. Therefore, there exists an intermediate roughness period at which the thermal conductivity reaches its minimum.

4. Conclusion

In this study, we have developed an improved wave reflection model for periodically rough surfaces that comprehensively accounts for both phase interference and directional deflection effects. By introducing a position-dependent reflected wave vector and projecting the phase contribution onto the mirror reflection direction, the proposed model extends the classical Ziman framework and offers a more physically accurate estimation of the specular reflection probability.

Our results demonstrate that increasing the roughness amplitude markedly suppresses specular reflection due to enhanced phase variation and increased surface inclination. Importantly, the model captures oscillatory features in the specularity at short phonon wavelengths, which arise from coherent interference effects similar to diffraction in periodic structures.

The enhanced reflection model is successfully integrated into Monte Carlo simulations of phonon transport. The simulation results reveal a non-monotonic

dependence of thermal conductivity on the roughness period: thermal conductivity is relatively high when the period is either very small or very large. This behavior is attributed to the reduced phonon sensitivity to fine features at small periods and diminished reflection-induced scattering at large periods due to lower surface slopes.

Overall, the proposed model provides new insights into the role of periodic roughness in phonon-boundary interactions and offers a more robust framework for predicting thermal transport in nanostructured materials.

Funding

This work was supported by the China Scholarship Council (No. 202308090243 for S. Liu and No. 202408090635 for F. Yin).

CRediT authorship contribution statement

Fei Yin: Methodology, Validation, Formal analysis, Investigation, Writing - original draft, Writing - review & editing. **Shixian Liu:** Methodology, Formal analysis, Writing - review & editing. **Alexander A. Barinov:** Methodology, Supervision, Writing - review & editing. **Vladimir I. Khvesyuk:** Conceptualization, Methodology, Supervision, Writing - review & editing.

Declaration of Competing Interest

The authors declare that they have no known competing financial interests or personal relationships that could have appeared to influence the work reported in this paper.

Acknowledgements

S. Liu and F. Yin gratefully acknowledges financial support from the China Scholarship Council (No. 202308090243 for S. Liu and No. 202408090635 for F. Yin).

Appendix A. Bessel Function Expression for Specular Amplitude

In this appendix, we provide the detailed derivation of the coherent specular amplitude from a periodically rough surface with sinusoidal height profile.

As described in Section 2, the position-dependent phase shift introduced by the surface is given by:

$$\Delta\varphi(x) = \frac{4\pi}{\lambda} h(x) \cos \theta = \frac{4\pi A \cos \theta}{\lambda} \sin\left(\frac{2\pi}{L}x\right). \quad (\text{A.1})$$

The coherent amplitude of specular reflection is obtained by averaging the complex phase factor over one period of the rough surface:

$$A_{\text{coh}} = \frac{1}{L} \int_0^L e^{i\Delta\varphi(x)} dx = \frac{1}{L} \int_0^L \exp\left[i\frac{4\pi A \cos \theta}{\lambda} \sin\left(\frac{2\pi}{L}x\right)\right] dx. \quad (\text{A.2})$$

Let us define a dimensionless parameter:

$$\alpha = \frac{4\pi A \cos \theta}{\lambda}, \quad (\text{A.3})$$

and perform a change of variable:

$$\phi = \frac{2\pi}{L}x \quad \Rightarrow \quad dx = \frac{L}{2\pi}d\phi.$$

Substituting into Eq. (A.2), we get:

$$A_{\text{coh}} = \frac{1}{2\pi} \int_0^{2\pi} e^{i\alpha \sin \phi} d\phi. \quad (\text{A.4})$$

This integral is a standard definition of the zeroth-order Bessel function of the first kind:

$$J_0(\alpha) = \frac{1}{2\pi} \int_0^{2\pi} e^{i\alpha \sin \phi} d\phi. \quad (\text{A.5})$$

Therefore, we obtain:

$$A_{\text{coh}} = J_0\left(\frac{4\pi A \cos \theta}{\lambda}\right). \quad (\text{A.6})$$

References

- [1] J. Hyun Oh, M. Shin, M.-G. Jang, Phonon thermal conductivity in silicon nanowires: The effects of surface roughness at low temperatures, *Journal of Applied Physics* 111 (4) (2012).
- [2] L. Maurer, S. Mei, I. Knezevic, Rayleigh waves, surface disorder, and phonon localization in nanostructures, *Physical Review B* 94 (4) (2016) 045312.
- [3] S. Neogi, J. S. Reparaz, L. F. C. Pereira, B. Graczykowski, M. R. Wagner, M. Sledzinska, A. Shchepetov, M. Prunnila, J. Ahopelto, C. M. Sotomayor-Torres, et al., Tuning thermal transport in ultrathin silicon membranes by surface nanoscale engineering, *ACS nano* 9 (4) (2015) 3820–3828.
- [4] D. L. Nika, A. S. Askerov, A. A. Balandin, Anomalous size dependence of the thermal conductivity of graphene ribbons, *Nano letters* 12 (6) (2012) 3238–3244.
- [5] H. Casimir, Note on the conduction of heat in crystals, *Physica* 5 (6) (1938) 495–500.
- [6] J. M. Ziman, *Electrons and phonons: the theory of transport phenomena in solids*, Oxford university press, 2001.
- [7] S. B. Soffer, Statistical model for the size effect in electrical conduction, *Journal of Applied Physics* 38 (4) (1967) 1710–1715.
- [8] S. Wolf, N. Neophytou, H. Kosina, Thermal conductivity of silicon nanomeshes: Effects of porosity and roughness, *Journal of Applied Physics* 115 (20) (2014).
- [9] M. Verdier, D. Lacroix, K. Termentzidis, Roughness and amorphization impact on thermal conductivity of nanofilms and nanowires: Making atomistic modeling more realistic, *Journal of Applied Physics* 126 (16) (2019).
- [10] M. Maldovan, Specular reflection leads to maximum reduction in cross-plane thermal conductivity, *Journal of Applied Physics* 125 (22) (2019).

- [11] S. Liu, A. A. Barinov, F. Yin, V. I. Khvesyuk, Determination of thermal properties of unsmooth Si-nanowires, Chinese Phys. Lett. 41 (2024) 016301.
- [12] S. Liu, Z. Zong, F. Yin, V. Khvesyuk, N. Yang, Quantifying particle and wave effects in phonon transport of pillared graphene nanoribbons, International Journal of Thermal Sciences 217 (2025) 110067.
- [13] J. Lim, K. Hippalgaonkar, S. C. Andrews, A. Majumdar, P. Yang, Quantifying surface roughness effects on phonon transport in silicon nanowires, Nano letters 12 (5) (2012) 2475–2482.
- [14] N. K. Ravichandran, H. Zhang, A. J. Minnich, Spectrally resolved specular reflections of thermal phonons from atomically rough surfaces, Physical Review X 8 (4) (2018) 041004.
- [15] A. Maznev, Boundary scattering of phonons: Specularity of a randomly rough surface in the small-perturbation limit, Physical Review B 91 (13) (2015) 134306.
- [16] C. Blanc, A. Rajabpour, S. Volz, T. Fournier, O. Bourgeois, Phonon heat conduction in corrugated silicon nanowires below the casimir limit, Applied Physics Letters 103 (4) (2013).
- [17] H. Chen, H. Wang, Y. Yang, N. Li, L. Zhang, Rough boundary effect in thermal transport: A lorentz gas model, Physical Review E 98 (3) (2018) 032131.
- [18] S. Tian, T. Wang, H. Chen, D. Ma, L. Zhang, Phonon coherent transport leads to an anomalous boundary effect on the thermal conductivity of a rough graphene nanoribbon, Physical Review Applied 21 (6) (2024) 064005.
- [19] Y.-X. Li, Specular transmission in nodal-line weyl semimetal resonant tunneling junction, Applied Physics Letters 117 (20) (2020).
- [20] S. G. Lipson, H. S. Lipson, D. S. Tannhauser, Optik, Springer-Verlag, 2013.
- [21] J.-P. M. Péraud, N. G. Hadjiconstantinou, Efficient simulation of multidimensional phonon transport using energy-based variance-reduced

monte carlo formulations, Physical Review B—Condensed Matter and Materials Physics 84 (20) (2011) 205331.

- [22] S. Liu, F. Yin, V. I. Khvesyuk, Investigating anisotropic three-phonon interactions in graphene's thermal conductivity using monte carlo method, International Journal of Thermophysics 46 (2) (2025) 1–19.
- [23] S. Mazumder, A. Majumdar, Monte carlo study of phonon transport in solid thin films including dispersion and polarization, J. Heat Transfer 123 (4) (2001) 749–759.
- [24] R. Anufriev, M. Nomura, Ray phononics: Thermal guides, emitters, filters, and shields powered by ballistic phonon transport, Materials Today Physics 15 (2020) 100272.
- [25] B. H. Silva, D. Lacroix, M. Isaiev, L. Chaput, Monte carlo simulation of phonon transport from ab-initio data with nano- κ , Computer Physics Communications 294 (2024) 108954.